On the selective transport of mixtures of organic and inorganic anions through anion-exchange membranes: A case study about the separation of nitrates and citric acid by electrodialysis

M.C. Martí-Calatayud [*], M. Ruiz-García, V. Pérez-Herranz

IEC Group, ISIRYM, Universitat Politècnica de València, Camí de Vera s/n, P.O. Box 22012, E-46071, 46022 València, Spain

ARTICLE INFO

ABSTRACT

Electrodialysis is finding an increasing number of applications, recently also in the separation and purification of organic acids. This technology involves reducing the use of chemicals and the generation of wastes, as compared to conventionally used processes. Gaining insights about the competitive transport between organic and inorganic ions in ED systems is key to achieving efficient separation processes in the bioresource industry. In the present study, the competitive transport of organic (citrates) and inorganic anions (nitrates) through anion-exchange membranes is investigated, under varying pH conditions, ion concentrations, and applied currents, by means of chronopotentiometry and ED experiments. In the absence of nitrate ions and under acidic conditions (pH 2), the resistance of the membrane system is very high because citric acid is mainly present in its undissociated and uncharged form. In the case of sodium citrate (pH 8), the membrane resistance decreases, especially at high current densities, which promote dissociation reactions and the subsequent concentration increase in ionic species near the membrane. Such phenomenon is identified both in chronopotentiometric curves and in long-term ED experiments by a gradual drop in membrane voltage with time. Although being less concentrated than citrates, the selective removal of nitrates is the most effective choice for the separation of both types of species. The selectivity factor of nitrates over citrates reaches the highest values at low applied current densities (below the limiting current density), with stable permselectivity values higher than 20. Such conditions also lead to the least specific energy consumption per nitrates removed ($<0.5\ kW\cdot hr\cdot kg_{NO_3^-}^{-1}$). Therefore, ED can be used under such favorable operating conditions after a clarification step in order to remove inorganic ions from fermentation broths and increase the purity of organic acids. At higher current densities, the enhanced transport of citrate anions produces a significant drop in selectivity towards nitrates and increases the specific energy consumption.

1. Introduction

An efficient transition from a petroleum-based economy to one mainly based on renewable feedstocks requires from the development of sustainable production routes that rely on bioresources. Organic acids occupy an important place among platform chemicals that could replace fossil fuels as commodities in industrial sectors [1]. They include C–C bonds and carboxylic functional groups in their structure, which makes feasible their conversion into a variety of high-demand derivatives. Short-chain organic acids (e.g. oxalic, malic, succinic, fumaric or citric acid) are especially relevant in the food sector and in the production, among others, of cosmetics, biodegradable plastics and pharmaceuticals [2].

Short-chain organic acids can be obtained via chemical synthesis, but also as the fermentation product of different substrates, such as sugars, molasses, or even from the cleavage of lignocellulosic biomass [2,3]. Citric acid is one of the organic acids that is predominantly produced by fermentation, with a global annual production that exceeds 2 million tons [4]. The yield and selectivity of fermentation processes can be optimized by adjusting multiple parameters, such as the pH value, the type of feedstock or the concentration of nutrients and metals in fermentation broths [4,5]. Some of the nutrients are usually composed of inorganic salts, such as phosphates or nitrates. After the enzymatic phase, downstream separation and purification steps are needed to

---

reach a final marketable product; these steps being key contributors to the overall process costs [6,7]. The most common process for citric acid recovery and purification is based on precipitation, where calcium hydroxide and sulfuric acid are added to obtain the final product. Such steps, apart from involving the use of large quantities of reagents, also result in the generation of sludge and solid wastes [8].

Membrane processes imply relevant advantages over traditional separation technologies like chemical precipitation or solvent extraction, as they can be coupled in different stages of production cycles and facilitate the isolation of the products of interest with a minimal addition of reagents [9,10]. Among membrane processes, electrodialysis (ED) is especially suited for the separation of ionic compounds. Previous works based on ED processes have demonstrated the technological feasibility of ED for the separation and purification of organic acids [11,12]. Hernandez et al. achieved a 60 % recovery of medium-chain organic acids from a mimicked fermentation broth using a conventional ED cell [13]. Also, the use of anion-exchange membranes in a two-chamber ED setup was proven effective for extracting short-chain carboxylates from fermenters and enable their subsequent conversion into volatile esters [10]. In a recent study, the selective separation of specific acids from mixtures of organic acids was tested using different types of anion-exchange membranes, and membrane properties and solution pH were found determining factors in the selective separation of acetate anions [14].

Usually, fermentation media include not only organic substrates and products, but also inorganic ions, such as nitrates, which are present in the feedstock or added as nutrients [15]. Thus, ED separation involves the simultaneous transport of weak and strong electrolytes, i.e. carboxylates and inorganic salts, through ion-exchange membranes. Preliminary investigations about transport of mixtures including organic acids highlight the specific selectivity of the membranes and the degree of ionization of the organic species, among others, as two factors affecting the separation process [16,17]. The electrolyte conductivity and the phenomenon of concentration polarization also have a strong impact on the energy required for the separation. Melnikov et al. evaluated the conductivity of different anion-exchange membranes submerged in solutions of mono-, di- and tri-valent carboxylic anions, identifying a behavior significantly different to that of the same membranes submerged in strong electrolytes; they found out that the external electrolyte concentration had a minor effect on the membrane conductivity [18]. Luiz et al. investigated the selective behavior of anion-exchange membranes during the separation of inorganic and organic ions present in three different molasses: they detected a trade-off between the separation of inorganic/organic ions and the energy consumption during ED tests [19]. Currently, the main strategy followed to separate organic and inorganic ions from complex mixture solutions is based on targeting the removal of inorganic ions from the desired concentrated organic acid solution, either by controlling the operating conditions or by tailoring the surface properties of ion-exchange membranes. Recently, Zhou et al. reported the successful concentration of hydrochloric acid from oxalic acid mother liquor by electrodialysis, achieving highly pure HCl (>91.5 %) in the receiving compartment [20]. In a similar strategy, Lin et al. developed a highly conducting anion-exchange membrane based on the co-deposition of dopamine and polyethyleneimine, which showcased recovery efficiencies for organic antibiotics present in highly concentrated NaCl solutions >99.1 % thanks to the selective removal of the inorganic salt [21]. In the same line, Kim et al. developed a highly selective polyelectrolyte membrane suitable for the effective separation of chloride ions from succinate concentrates, which were then fed to an organic acid crystallization process [22].

In addition to the relevance of membrane selectivity towards different types of ions on the separation process, carboxylic acids can participate in ampholytic reactions, which involve changes in ion transport through the membranes during an ED process. In this line, Gorobchenko et al. identified experimentally and by modeling studies that several limiting current densities may arise in current–voltage curves of systems involving polybasic acids [23,24]. Moreover, a similar phenomenon was identified by electrochemical impedance measurements in phosphate solutions by Rotta et al., where this phenomenon was related to ampholytic reactions that were tracked by the registration of Gerischer arcs in the impedance spectra [25]. Apart from the identification of such reactions in short-term experiments, their relevance in long-term ED has not been addressed in depth.

In this work, the separation of citric acid and nitrate ions in ED systems using homogeneous AMV-N anion-exchange membranes is investigated. Various aspects related to the organic acid synthesis and purification processes, like the electrolyte pH, the presence of competing inorganic anions typically present as nutrients, and the regime of applied current density in an ED cell are considered. A preliminary study of the membrane behavior has been conducted to identify the current density regimes for different electrolyte systems by means of short-term electrochemical characterization techniques. Subsequently, the evolution of the voltage drop and the nitrate-to-citrate selectivity have been evaluated in ED tests of longer duration. Such tests allowed the authors to identify significant changes in membrane selectivity and energy consumption during the progress of ion transport under an imposed electric field.
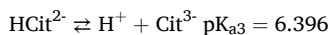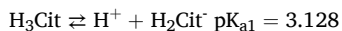
2. Experimental

2.1. Reagents, membranes and electrodialysis setup

Citrate and nitrate have been selected as model species to study the transport of organic and inorganic anions in ED systems. Synthetic solutions were prepared using reagents of analytical grade (Panreac) and Type 1 Milli-Q ultrapure water. Tri-sodium citrate 2-hydrate ($Na_3C_6H_5O_7 \cdot 2H_2O$), citric acid ($C_6H_8O_7$) and sodium nitrate ($NaNO_3$) were used as reagents.

Based on the concentration of citric acid achieved in fermentation reactors, two different levels of citrate concentration have been investigated, 0.1 M and 0.05 M [26–28]. Moreover, depending on the specific conditions of the citric acid production process, the optimum bioreactor pH may vary significantly [5,29,30]. Accordingly, solutions at two pH levels were prepared: citric acid, with a pH value around 2, and sodium citrate, with a pH value around 8. The presence of a competing inorganic anion was considered by preparing mixtures with sodium nitrate, which is usually dosed in fermenters as a source of nitrogen [31,32]. Table 1 shows a summary of the different solutions investigated in this study and their characteristics. In the following lines, the citrate anion ($C_6H_5O_7^{3-}$) will be referred to as Cit^{3-}.

Table 1
Solutions used in the electrochemical experiments and their characteristic properties.

Solution	Citrate concentration	pH level	Presence of competing ion
0.1 M H₃Cit	High	Low	No
0.1 M H₃Cit + 0.015 M NaNO₃		(~2)	Yes
0.1 M Na₃Cit		High	No
0.1 M Na₃Cit + 0.015 M NaNO₃		(~8)	Yes
0.05 M H₃Cit	Low	Low	No
0.05 M H₃Cit + 0.015 M NaNO₃		(~2)	Yes
0.05 M Na₃Cit		High	No
0.05 M Na₃Cit + 0.015 M NaNO₃		(~8)	Yes

Citric acid can undergo up to three deprotonation steps according to the following reactions [33]:

$$H_3Cit \rightleftharpoons H^+ + H_2Cit^- \quad pK_{a1} = 3.128$$

$$H_2Cit^- \rightleftharpoons H^+ + HCit^{2-} \quad pK_{a2} = 4.761$$

$$HCit^{2-} \rightleftharpoons H^+ + Cit^{3-} \quad pK_{a3} = 6.396$$

The distribution of ions in citrate solutions as a function of the pH value are shown in Fig. 1, where the dotted lines represent the initial pH

conditions of each solution. For the sake of conciseness, only the speciation diagrams of the solutions having a concentration of citrates of 0.1 M (either prepared from the citric acid or from the salt) are shown. Speciation diagrams for mixtures with a citrate concentration of 0.05 M are included in Fig. A.1 of the Appendix section. In 0.1 M H_3Cit solutions (pH 2, Fig. 1 a and b), citrates are mainly in the form of the undissociated acid H_3Cit. Monovalent H_2Cit^- anions are also present, but at concentrations lower than 0.01 M. In mixtures with $NaNO_3$ at pH 2 (Fig. 1 b), the anion with the highest concentration is NO_3^-. With regards to the 0.1 M Na_3Cit solutions prepared from the salt, which have a pH value of 8
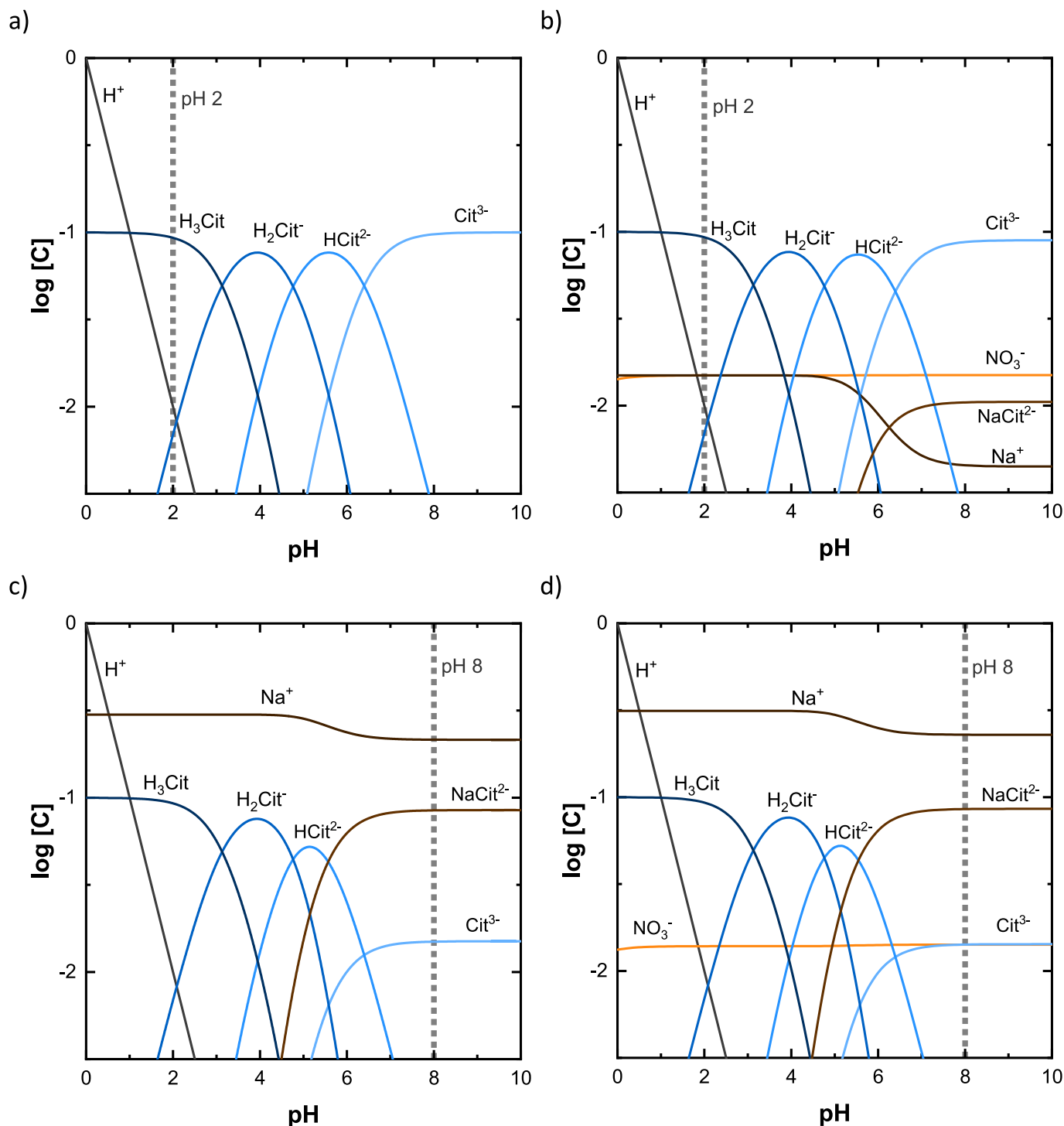

Fig. 1. Logarithmic concentration diagram for (a) 0.1 M H_3Cit, (b) mixtures of 0.1 M H_3Cit and 0.015 M $NaNO_3$, (c) 0.1 M Na_3Cit and (d) mixtures of 0.1 M Na_3Cit and 0.015 M $NaNO_3$.
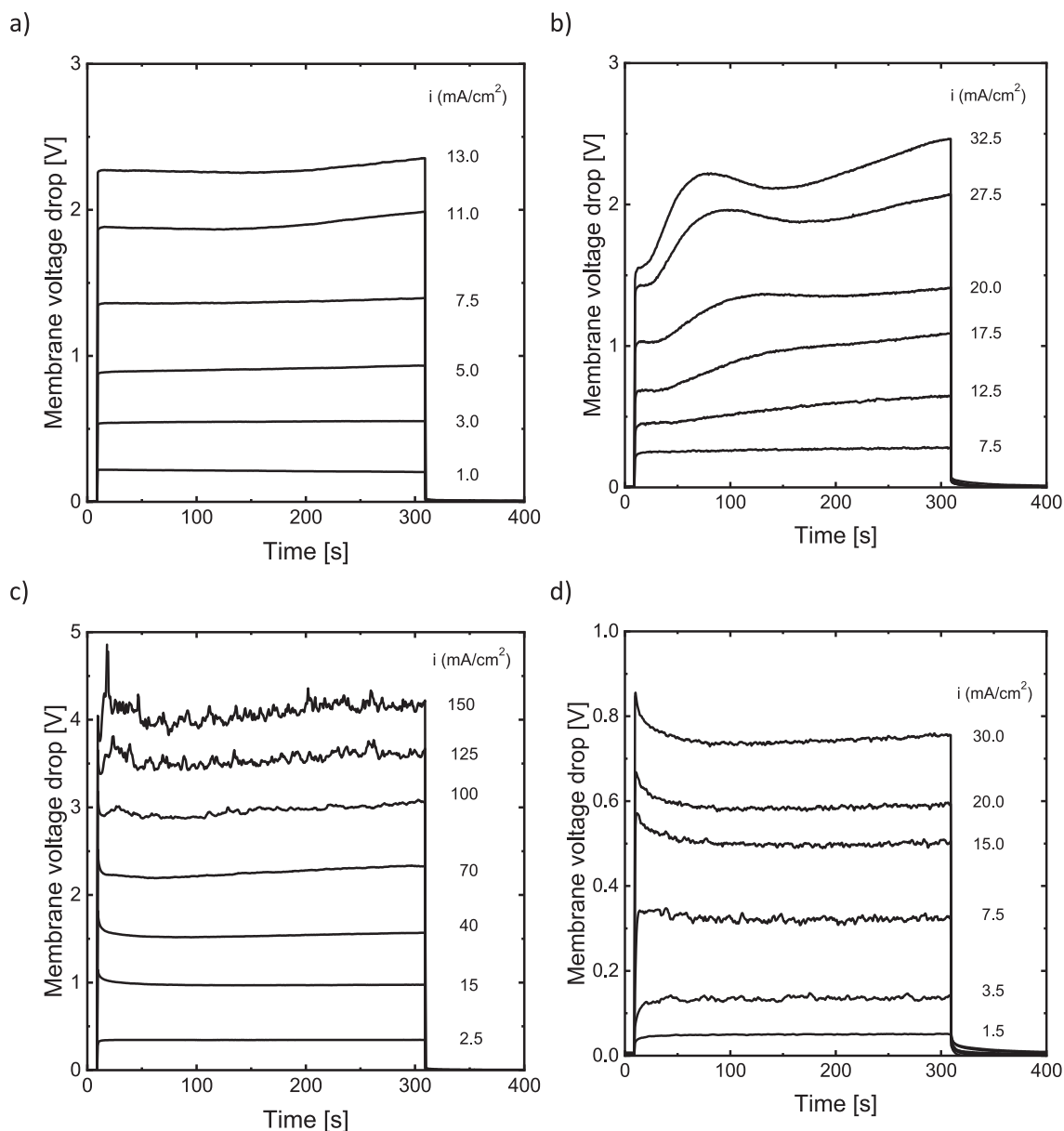
Fig. 2. Chronopotentiometric curves obtained with (a) 0.1 M H$_3$Cit, (b) mixtures of 0.1 M H$_3$Cit 0.1 M and 0.015 M NaNO$_3$, (c) 0.1 M Na$_3$Cit and (d) mixtures of 0.1 M Na$_3$Cit and 0.015 M NaNO$_3$.

(Fig. 1 c and d), the divalent NaCit^{2-} anion predominates in solution, followed by trivalent Cit^{3-} anions with a concentration close to 0.015 M. Moreover, in the mixtures, the concentration of NO$_3^-$ is very similar to that of Cit^{3-} anions (Fig. 1 d).

AMV-N anion-exchange membranes were used in the present study (Selemion, AGC Engineering, Japan). AMV-N has an homogeneous structure and presents quaternary amines as the main charged group, introduced by grafting in the membrane matrix. The membranes have a thickness between 80 and 120 μm and an ion-exchange capacity of 1.85 meq/g [34]. Nafion 117 cation-exchange membranes were used as separators for the cathodic compartment.

An ED cell formed by three compartments was employed for conducting chronopotentiometric and electrodialysis experiments. This cell has been presented and described in detail in some of our previous studies [35,36]. The membrane under study, AMV-N, was placed between the anodic and the central compartment, while the Nafion 117 membrane was used to separate the central and the cathodic compartment. Each compartment has a volume capacity of 125 ml and was

stirred with a magnetic stirrer at 400 rpm. The electrochemical measurements were conducted using the four-point method. Graphite bars connected to the power source were used as electrodes, and the membrane voltage drop was measured via two Ag/AgCl reference electrodes immersed in Luggin capillaries. These were installed at each side of the AMV-N membrane with their tips placed at approximately 1 mm from the membrane surface.

2.2. Electrochemical measurements

The dynamics of ion transport through the anion-exchange membrane were studied by means of chronopotentiometry. This technique is based on the measurement of the voltage drop across the membrane system during the application of current pulses. For each electrolyte (Table 1), several current pulses were applied in order to investigate the transport of ions at different current regimes. The current was applied during 300 s, and then, the system was monitored during 100 additional seconds until the initial equilibrium voltage drop could be reestablished

[37]. The anode and cathode were connected to an Autolab PGSTAT302 N galvanostat/potentiostat, that was used as the power supply, and the voltage drop between the tips of both Luggin capillaries was registered. During the chronopotentiometric experiments, the membrane area was reduced to 1 cm^2 to limit the changes in concentration in each compartment and to allow reaching overlimiting current densities within the measurement range allowed by the galvanostat. All experiments were conducted at room temperature (25 °C).

The current–voltage curves for each electrolyte system were obtained by plotting the final values of membrane voltage drop of each chronopotentiogram against their respective applied current density. As a result, an overview of the regimes of ion transfer through the membrane can be obtained for the different electrolytes investigated. The limiting current density (i_{lim}) of each system can also be determined from the current–voltage curves.

2.3. Electrodialysis experiments

Once the transport of anions through the membranes was characterized, electrodialysis experiments were conducted in galvanostatic mode using a membrane area of 12.56 cm^2 and the mixtures with the highest citrate concentration: 0.1 M H$_3$Cit + 0.015 M NaNO$_3$ (pH 2) and 0.1 M Na$_3$Cit + 0.015 M NaNO$_3$ (pH 8). The values of current density were selected based on the current–voltage curves previously obtained, as it is explained below in section 3.2 (i_1 = 2.5, i_2 = 7.5 and i_3 = 12 mA/cm^2). The electrodialysis experiments were conducted for 4 h and samples were taken from the central (diluate) compartment at least every 30 min to evaluate the evolution of the concentration of citrate and nitrate anions. At specific times, samples were also collected from the concentrate compartment (anolyte). The evolution of pH in each compartment and the final values of conductivity were also measured.

The concentration of Cit^{3-}-containing species in each sample was obtained by measuring the concentration of total organic carbon (TOC), using a Shimadzu TNM-L ROHS TOC analyzer. The concentration of NO$_3^-$ and Na$^+$ ions was measured using a Metrohm Ionic Chromatograph 883 Basic IC Plus.

The flux of citrates ($J_{Cit^{3-}}$) and nitrates ($J_{NO_3^-}$) through the anion-exchange membrane was calculated according to the following equations [38]:

$$J_{Cit^{3-}} = \frac{V \frac{dC_{Cit^{3-}}}{dt}}{A_m} \tag{1}$$

$$J_{NO_3^-} = \frac{V \frac{dC_{NO_3^-}}{dt}}{A_m} \tag{2}$$

where V represents the volume of the central compartment, $c_{Cit^{3-}}$ and $c_{NO_3^-}$ represent the concentration at each time of Cit^{3-} and NO$_3^-$, respectively, and A_m represents the membrane area.

The selectivity of the process towards the transport of NO$_3^-$ ions over that of Cit^{3-} species was evaluated by calculating their relative permselectivity factor according to the following equation:

$$P_{Cit^{3-}}^{NO_3^-} = \frac{J_{NO_3^-}/C_{NO_3^-}}{J_{Cit^{3-}}/C_{Cit^{3-}}} \tag{3}$$

As can be seen in Eq. (3), each flux is divided by the respective ion concentration. This normalization is particularly relevant in this research because the concentration of citrate species in the solutions is significantly higher than that of nitrates (see Table 1 and Fig. 1).

The specific energy spent in the membrane system to transfer nitrate ions through the membranes, $E_{s,m}$, was also calculated from the evolution of membrane voltage (U_m) over time, using Eq. (4),

$$E_{s,m} = \frac{\int_0^t I \bullet U_m dt}{(C_{NO_3^-,0} - C_{NO_3^-}) \bullet V \bullet M_{NO_3^-}} \tag{4}$$

where I represents the applied current, $c_{NO_3^-,0}$ and $M_{NO_3^-}$ the initial concentration and the molar mass of nitrate ions.

3. Results and discussion

3.1. Chronopotentiometric response

The chronopotentiograms obtained for solutions at the high level of citrate concentration are shown in Fig. 2. In the case of 0.1 M H$_3$Cit solutions (pH 2, Fig. 2 a), the chronopotentiometric response is very flat, even though the potential drop reaches values higher than 2 V. In each chronopotentiogram, when the current application starts, the ohmic voltage drop of the system is established instantaneously. Then, this initial value remains almost constant during the 300 s of the pulse. This response is the expected one at low values of current density, when diffusive transport in the solution compensates the difference in anion migration flux between the membrane and the solution. However, as the driving force for migration increases (i.e. at increasing current densities), the difference between the anion migration flux in the membrane and in the solution also increases. At high current densities, the supply of ions towards the membrane surface facing the dilute compartment becomes limited by diffusion. This phenomenon usually results in the formation of concentration gradients near the membrane, what is commonly known as concentration polarization. The depletion of counter-ions near the dilute surface of a membrane can be tracked by an almost vertical increase in the voltage drop during the chronopotentiometric measurements [37]. In the chronopotentiograms of Fig. 2 a, although values of membrane voltage drop higher than 2 V were reached, no remarkable increments in the membrane voltage drop were registered during the tests.

A different response was obtained for mixtures of H$_3$Cit and NaNO$_3$ (Fig. 2b). The development of concentration polarization is clearly manifested in the form of an increase in voltage drop at high current densities. For example, for 27.5 mA/cm^2, the membrane voltage drop increases approximately 25 s after the current is applied. This notorious increase in voltage drop confirms the progressive depletion of ions at the dilute side of the membrane. Considering the different responses obtained for the citric acid solution with and without nitrate, the increase in voltage drop observed with the mixtures can be attributed to the depletion of nitrate ions near the membrane surface. In effect, as can be seen in the speciation diagrams of Fig. 1b, the concentration of nitrate ions is higher than that of any organic anion present in solution at pH 2. At low pH values, citric acid is mainly in the form of the undissociated form of the acid H$_3$Cit, which, as an uncharged specie, should not be affected by the imposed electric field. The curves registered with the mixture resemble those typically obtained with strong electrolytes; as an example, the chronopotentiograms obtained for 0.1 M NaCl are shown for comparison purposes in Fig. A.2 (Appendix section).

The chronopotentiograms obtained with the 0.1 M Na$_3$Cit salt solution (pH 8, shown in Fig. 2 c) are similar to those obtained with 0.1 M H$_3$Cit. However, two distinctive features can be observed at certain levels of current density. The first feature is observed for current densities between 15 and 70 mA/cm^2, where an initial peak and subsequent decrease in voltage is registered in the first part of the chronopotentiograms. The second feature can be seen when higher current densities are applied (100–150 mA/cm^2): after the initial peak, a slight increase in voltage drop takes place during the first seconds of the chronopotentiograms. As mentioned above, the increase in membrane voltage can be caused by the development of concentration profiles in the diffusion boundary layers, as a consequence of the transport of anions (in this case, mainly NaCit^{2-} and Cit^{3-}) taking place faster through the membrane than within the solution. After this small increase, the voltage oscillates around an average value. The oscillations in voltage drop are usually attributed to the generation of fluid vortices by electroconvection. Electroconvection emerges at an advanced stage of

Table 2
Conductivity of pH of the different 0.1 M citrate solutions used in the present study.

	0.1 M H$_3$Cit	0.1 M H$_3$Cit + 0.015 M NaNO$_3$	0.1 M Na$_3$Cit	0.1 M Na$_3$Cit + 0.015 M NaNO$_3$
Conductivity (mS/cm)	3.35	4.72	18.31	17.03
pH	2.09	2.13	8.44	7.95

concentration polarization when high current densities are applied and the concentration of ions near the depleting membrane surface becomes close to zero. Electroconvective vortices provide an additional mixing in the diffusion boundary layer and generate local changes in electrolyte concentration that result in the observed oscillations in the measured potential [39–41].

For the 0.1 M Na$_3$Cit and 0.015 M NaNO$_3$ mixtures (pH 8, Fig. 2 d), an increase of voltage drop can already be seen in the first part of the chronopotentiograms for current densities lower than 7.5 mA/cm^2. It seems that depletion of NO$_3^-$ ions from the dilute membrane surface takes place at low current densities, while that of citrate species takes place at higher current densities, as observed for 0.1 M Na$_3$Cit at i > 70 mA/cm^2. In the case of the mixtures with nitrate, the increase in voltage drop observed at low current densities is much smaller at pH 8 than at pH 2 (Fig. 2 b). According to the speciation diagrams for the mixtures at pH 8 (Fig. 1 d), NO$_3^-$ is not the most concentrated anion in solution and other ions, such as Cit^{3-}, also contribute to the solution conductivity. This would explain that an early depletion of NO$_3^-$ ions only causes a slight increase in the voltage drop, because the concentration of Cit^{3-} ions available in the diffusion boundary layer is still significant. On the contrary, with the mixtures of H$_3$Cit and NaNO$_3$ (speciation diagram of Fig. 1 b), NO$_3^-$ is the most concentrated anion in the electrolyte, while the contribution of citrate species to the electrolyte conductivity is almost negligible, as they are in the form of the uncharged molecule H$_3$Cit. Consequently, the different contribution of NO$_3^-$ ions to the total solution conductivity as a function of pH would explain the larger magnitude of
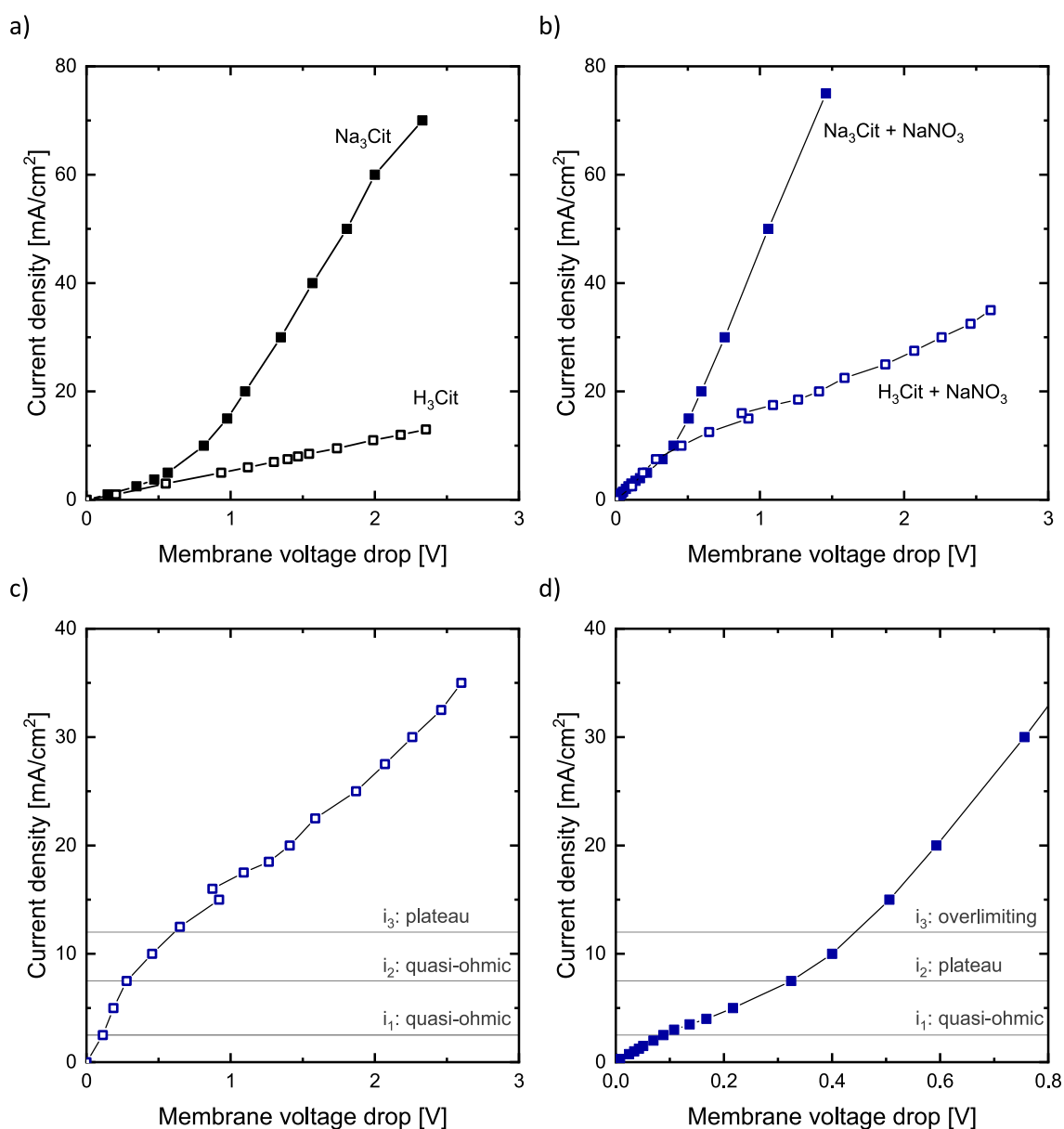

Fig. 3. Current-voltage curves (a) comparison between single solutions of 0.1 M Na$_3$Cit and 0.1 M H$_3$Cit, (b) comparison between mixtures of 0.1 M H$_3$Cit + 0.015 M NaNO$_3$ and mixtures of 0.1 M Na$_3$Cit + 0.015 M NaNO$_3$, (c) Zoom of curve obtained with 0.1 M H$_3$Cit + 0.015 M NaNO$_3$, and (d) Zoom of curve obtained with 0.1 M Na$_3$Cit + 0.015 M NaNO$_3$.

the increase in membrane voltage drop registered with the mixtures at pH 2. In effect, the measured conductivities shown in Table 2 for each system reveal that the addition of NaNO$_3$ to H$_3$Cit solutions increases conductivity, while it causes the reverse effect in the case of Na$_3$Cit solutions. In Fig. 1 d, at current densities above 15 mA/cm^2, the initial peak and subsequent decline of membrane voltage drop also appears in the chronopotentiograms, similar to what was observed in the absence of NaNO$_3$. This feature is discussed in more detail in section 3.2.

The chronopotentiograms obtained for the low level of citrate concentration (0.05 M) exhibited a very similar evolution to that described for 0.1 M solutions, hence revealing that the effect of the electrolyte concentration on the electrochemical response of the system is less important than those related to the solution pH and the presence of inorganic NO$_3^-$ ions in solution. These results can be seen in Fig. A.3 (Appendix section).

3.2. Current-voltage curves

The current–voltage curves obtained for the different electrolyte systems at a total citrate concentration of 0.1 M are shown in Fig. 3. In agreement with the flat chronopotentiograms shown above in Fig. 1 a, the current–voltage curve obtained for 0.1 M H$_3$Cit is linear, including only one region of almost constant resistance for the range of current densities investigated. In contrast, the current–voltage curve obtained with 0.1 M Na$_3$Cit shows two different regions: one at low current densities denoting a high resistance to ion transport (smaller slope) and a second one above 10 mA/cm^2 of decreased resistance (larger slope). It must be emphasized that this behavior is quite different from that observed with strong electrolytes, where, as the current density increases, the membrane resistance also increases, usually preceding a plateau region associated with a fully developed concentration polarization (cf. Fig. A.2b in the Appendix, corresponding to NaCl solutions as an example of a strong electrolyte).

By comparing the shape of the chronopotentiograms and the current–voltage curves, one can identify that the registration of initial peaks in the chronopotentiograms (Fig. 2 c) corresponds with the decrease in membrane resistance observed at current densities higher than 10 mA/cm^2 (Fig. 3 a). This uncommon feature has also been reported by Pismenskaya et al. in systems formed by homogeneous Neosepta AMX membranes with NaH$_2$Cit solutions at a pH value of 4 [42]. In that study, the large resistance observed at low values of current density was attributed to the accumulation of uncharged H$_3$Cit molecules in the diffusion boundary layer, while the decrease in resistance at higher currents was assigned to the progressive deprotonation of HCit^{2-} ions into trivalent Cit^{3-} ions in the membrane phase. In the same line, Stodollick et al. registered current–voltage curves of decreasing resistance at high currents with a system formed by homogeneous Fumasep membranes in contact with mixtures of itaconic acid (C$_5$H$_6$O$_4$) and sodium chloride [43]. In the present study, the dissociation of NaCit^{2-} giving rise to Cit^{3-} and Na$^+$ ions can also occur in the membrane, increasing the ionic charge transported by citrate species through the membrane and supplying Na$^+$ ions to the depleting diffusion boundary layer. This phenomenon would explain the atypical evolution of membrane resistance with the applied current density for Na$_3$Cit solutions.

As reported in a previous study, the dissociation of complex species in membrane systems can be accelerated at high current densities by the increased Donnan exclusion for co-ions as the solution layer adjacent to the membrane becomes more diluted in ionic species [44]; but also by the higher intensity with which co-ions become attracted towards the cathode (in the present case). Related to this effect, previous studies have also revealed that dissociation constants of weak electrolytes in ion-exchange membranes can be up to 10 times higher than in aqueous solutions [45]. The membrane properties seem to play a role in this phenomenon, since the chronopotentiometric and current–voltage curves registered with heterogeneous membranes and Na$_3$Cit solutions in a previous study do not exhibit a decrease in resistance at increasing
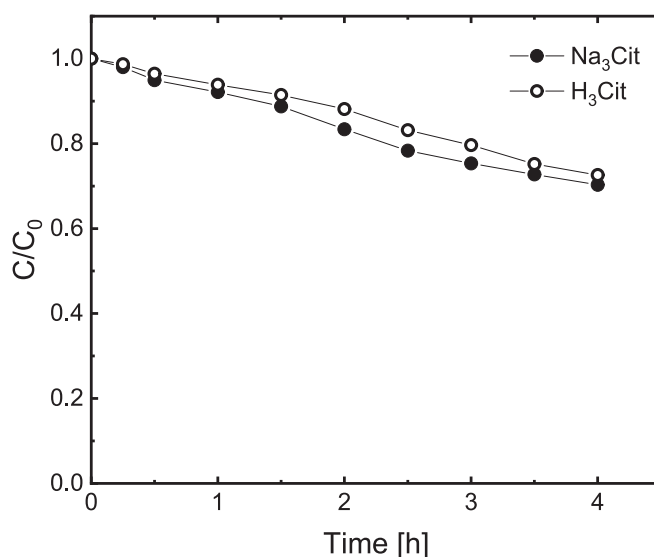

Fig. 4. Evolution of the relative citrate concentration (C/C$_0$) under the application of a current density of 7.5 mA/cm^2 for 0.1 M H$_3$Cit and 0.1 M Na$_3$Cit solutions.

currents [46], differing significantly from the results presented in this work. Regarding the effect of solution pH on the development of dissociation reactions, the peaks in voltage drop are more notorious with the salt solutions (pH 8). However, by looking at the chronopotentiograms shown in Fig. A.3a, the same phenomenon is also detected for 0.05 M H$_3$Cit solutions (pH 2). These results reveal that the undissociated acid molecule H$_3$Cit and the H$_2$Cit$^-$ anion can also undergo deprotonation reactions near the membrane. The fact that deprotonation reactions become more important at low H$_3$Cit concentrations reinforces the idea that the Donnan effect is the main phenomenon triggering the dissociation of complex species near ion-exchange membranes. H$^+$ ions are more mobile than Na$^+$ ions and can easily penetrate into the anion-exchange membrane; this resulting in an easier repulsion for Na$^+$ ions by the membrane matrix as compared to protons. Moreover, the capability of the membranes to exclude H$^+$ ions is expected to increase at lower concentrations, thus explaining the decrease in membrane resistance observed at increasing currents for 0.05 M H$_3$Cit solutions, but not for 0.1 M H$_3$Cit.

The current–voltage curves obtained for the mixtures (Fig. 3 b) exhibit three characteristic regions: a quasi-ohmic region of low resistance, a plateau region appearing when the corresponding i$_{lim}$ is reached, and a decrease in membrane resistance at overlimiting currents. In addition to the three characteristic regions, it is to note that the decrease in resistance detected for the 0.1 M Na$_3$Cit system at current densities higher than 10 mA/cm^2 is also observed for the mixtures of Na$_3$Cit and NaNO$_3$; it already falls within the range of overlimiting currents (i > i$_{lim}$). To better identify the values of i$_{lim}$, a separate zoom of the curves for the pH 2 and pH 8 is presented in Fig. 3 c and d. According to the previous discussion, the registration of a limiting current density is associated with the presence of NO$_3^-$ ions in the mixtures; therefore, the i$_{lim}$ value indicates the current density at which NO$_3^-$ ions become practically depleted near the membrane surface. Above the i$_{lim}$, the transmembrane current should be carried mainly by citrate species. The i$_{lim}$ values are 9.3 mA/cm^2 for 0.1 M H$_3$Cit + 0.015 M NaNO$_3$ mixtures (pH 2) and 2.8 mA/cm^2 for 0.1 M Na$_3$Cit + 0.015 M NaNO$_3$ mixtures (pH 8). The higher i$_{lim}$ value registered for the mixtures at pH 2 may stem from the fact that the uncharged H$_3$Cit accumulate at the diffusion boundary layer, ensuring a larger supply of citrate species towards the membrane surface as they dissociate and delaying the depletion of nitrates.

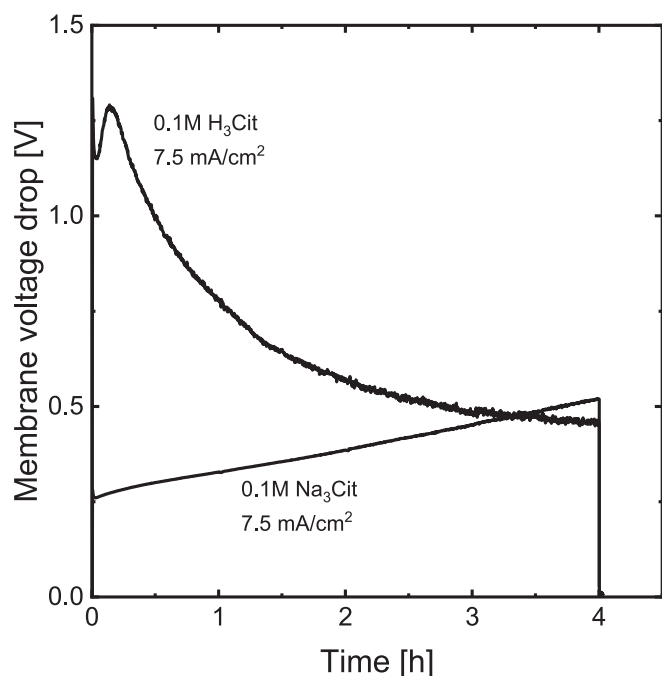As observed with the chronopotentiograms, the polarization curves

Fig. 5. Evolution of the membrane voltage drop under the application of a current density of 7.5 mA/cm² for 0.1 M H₃Cit and 0.1 M Na₃Cit solutions.
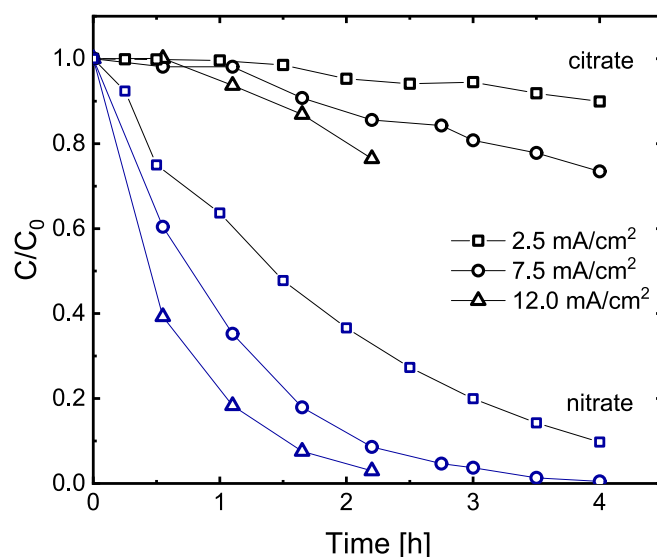

Fig. 6. Evolution of the relative concentration of citrates and nitrates (C/C₀) at different current densities for mixtures of 0.1 M H₃Cit and 0.015 M NaNO₃.

obtained with solutions more diluted in citrates are similar to those obtained for 0.1 M solutions (cf. Fig. A.4). Consequently, the ED experiments were conducted only with the high level of citrate concentration. The mixture solutions were selected to evaluate the selectivity factor between nitrates and citrates during the progress of ED experiments. Three different levels of current density were selected: $i_1 = 2.5$, $i_2 = 7.5$ and $i_3 = 12$ mA/cm². Each current density corresponds to three different regions of the current–voltage curve obtained for the mixtures at pH 8, as indicated by horizontal lines in Fig. 3 d. Since the values of i_{lim} are different for both systems, the two lowest values of current density fall in the quasi-ohmic region for the system at pH 2, and the highest value belongs to the plateau region.

3.3. Electrodialysis experiments

The effect of pH level, and consequently the distribution of species, on the transport of citrates through the anion-exchange membrane was further investigated with the single salt solutions 0.1 M H₃Cit and 0.1 M Na₃Cit. For this purpose, the central value of current density of 7.5 mA/cm⁻² (i_2) was selected. The relative concentration of citrate species with respect to the initial concentration (C/C₀) is shown in Fig. 4. The evolution of C/C₀ showcases a constant decay with time in both systems. The average flux of citrates was calculated from the linear fitting of the curves. A value of 0.192 mmol/(m²·s) was obtained for 0.1 M H₃Cit solutions, and a value of 0.212 mmol/(m²·s) was obtained for 0.1 M Na₃Cit, what reveals that, the transport efficiency of citrate species in the absence of competing inorganic anions is not affected by the solution pH. Despite the low concentration of negatively charged species at pH 2 (see Fig. 1 a) in comparison with the system at pH 8 (see Fig. 1 b), the flux of citrates through the membrane is almost the same. This trend

supports the hypothesis that, under the application of a constant current, dissociation reactions take place in both systems and the actual species permeating trough the membrane are the Cit³⁻ anions regardless of the pH value and solution speciation in the bulk.

Despite the similar flux of citrate species obtained with both systems, the evolutions of membrane voltage differ significantly, as shown in Fig. 5. The initial values of membrane voltage drop are very high for the solutions at pH 2, as expected from the low concentration of charged species and the low electrolyte conductivity at this pH (see Table 2). The differences observed at the beginning of the ED experiments as a function of pH show a good agreement with the current–voltage curves presented in Section 3.2. However, the evolution during the experiment is reversed for the two electrolytes. In the case of 0.1 M Na₃Cit, the evolution of the membrane voltage was the expected one: as the concentration of citrate species in the dilute compartment decreases with time, the resistance to current transfer and, consequently, the voltage drop increase. On the contrary, in the case of 0.1 M H₃Cit, the membrane voltage drop reaches a maximum of 1.25 V after approximately 10 min and then decreases continuedly until reaching a final value below 0.5 V. Despite this changing trend in membrane voltage, the flux of citrates remained constant during the experiment, what proves that the variations in membrane voltage are not related to a change in the main species being transported across the membrane.

At pH 2, the galvanostatic control of the ED system via the transport of citrate species can only be ensured if these are continuously generated from the H₃Cit molecules accumulated near the membrane. Hence, it seems that the dissociation phenomenon also takes place under a system that is polarized over longer times. Unlike the flat response observed in the chronopotentiograms for 0.1 M H₃Cit solutions, the ED experiments revealed that ampholytic reactions taking place in the salt solutions can also occur at acidic pH values, thus ensuring the supply of citrate anions to the membrane surface. From the continuous decrease in membrane voltage, we can infer that, the products of the dissociation reactions increase the conductivity of the diffusion boundary layer at the
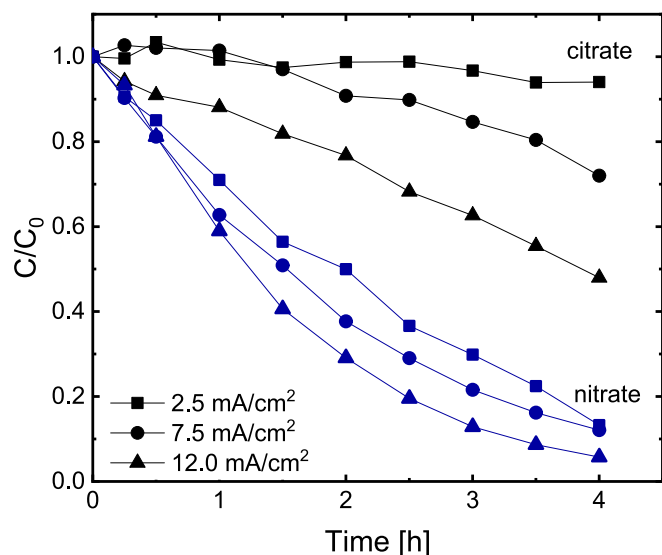
Table 3
Equivalent ionic conductivity and diffusion coefficient at infinite dilution for the main species involved in the dissociation of Na₃Cit and H₃Cit. Values obtained from [47].

	NO₃⁻	1/3 Cit³⁻	H₂Cit⁻	H⁺	Na⁺
Equivalent Conductivity (m²·S/mol)	71.42·10⁻⁴	70.2·10⁻⁴	30·10⁻⁴	349.65·10⁻⁴	50.08·10⁻⁴
Diffusion coefficient (cm²/s)	1.902·10⁻⁵	0.623·10⁻⁵	0.799·10⁻⁵	9.311·10⁻⁵	1.334·10⁻⁵

Fig. 7. Evolution of the relative concentration of citrates and nitrates (C/C$_0$) at different current densities for mixtures of 0.1 M Na$_3$Cit + 0.015 M NaNO$_3$.

conductivity of Cit^{3-} ions that permeate through the membrane leaving the diluted compartment (Table 3).

The evolution of the relative concentration of citrate species and nitrate ions during the ED experiments conducted with the mixture solutions are shown in Figs. 6 and 7. The first observation that can be made for the mixture solutions at both values of pH is that the concentration of citrates follows a linear decrease, while the concentration of nitrates decreases exponentially until reaching final values very close to zero. Here is to note that the initial concentration of nitrates is significantly lower than the total concentration of citrate species. However, this does not imply a limitation in the supply of nitrates from the bulk solution towards the membrane surface during the first stages of the experiments. For the solutions at pH 2 (Fig. 6), in line with the chronopotentiometric (Fig. 2 b) and current–voltage curves (Fig. 3 c), it can be confirmed that the transport of nitrate ions takes place preferentially, and these ions become depleted faster than citrates. Regarding the evolution of citrate species in the system, the decrease of concentration is very slow at the initial times, and it becomes accelerated when the concentration of nitrates has already decreased significantly. This change in slope is observed after 30 min of ED for a current density of 12 mA/cm^2, and after the first hour of ED for 7.5 mA/cm^2, which coincides with the time at which the relative concentration of nitrate ions reached a value lower than 0.4 and started to follow an asymptotic trend. For these two current densities, at the mentioned times, the supply of nitrates to the membrane surface becomes limited by mass transfer and enhances the transport of citrates towards the end of the ED experiment. In general, the increase in current density accelerates the decrease in concentration of both citrate and nitrate ions.

The results with the mixtures at pH 8 are analogous to the ones obtained at pH 2. Nevertheless, the transport of nitrate ions through the anion-exchange membrane is faster at pH 2, as can be inferred, for example, from the comparison of the results at the highest applied current density of 12 mA/cm^2: for the solutions at pH 2, the concentration of NO$_3^-$ ions reaches a value practically equal to zero after the two hours of experiment, while it takes the four hours of ED to reach similar values with the system at pH 8. From the general trends observed for both organic and inorganic species, it can be already inferred that it compensates to work at current densities below the i$_{lim}$ to achieve an effective separation of nitrates and citrates, because the concentration of the former decreases fast at low current densities, while the transport of citrate species remains very slow.
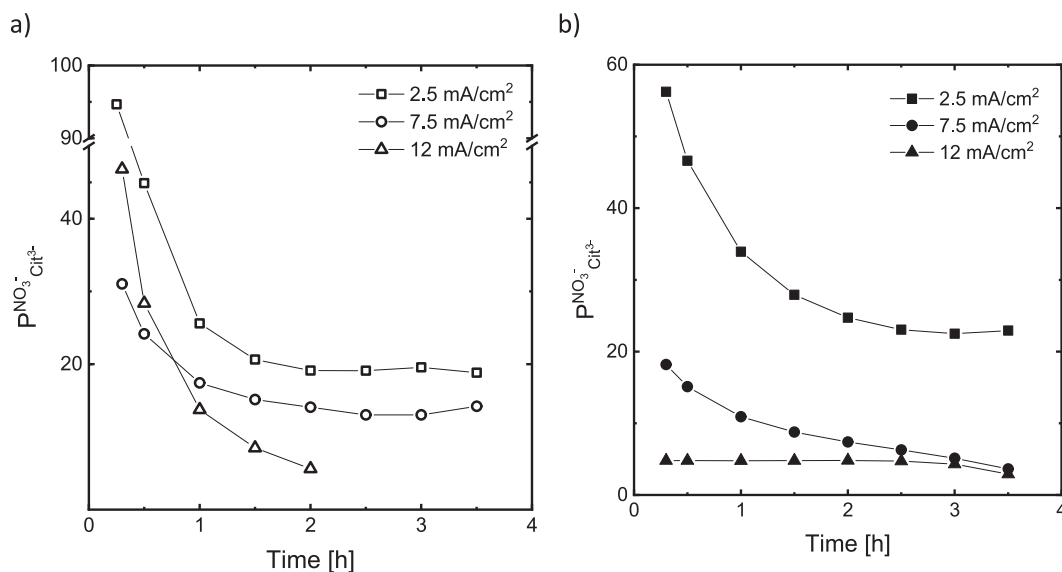
depleting side of the membrane. The dissociation of H$_3$Cit near the membrane surface at the dilute side implies the release of Cit^{3-} anions that are transported through the membranes, and also the release of H$^+$ ions. The latter contribute to increase the solution conductivity near the membrane in the diluted compartment. The equivalent conductivities of the ions involved in the dissociation reactions are summarized in Table 3. Note that the ionic conductivity of H$^+$ ions is the highest one, so the release of three protons per each dissociated H$_3$Cit molecule explains the significant drop in membrane voltage drop. The time needed for the release of a significant number of H$^+$ ions that would originate the decrease in membrane voltage is longer than the duration of the chronopotentiometric experiments, thus making it unfeasible to detect this phenomenon in the results shown in Fig. 2 a. In the case of 0.1 M Na$_3$Cit, the release of Na$^+$ ions as a consequence of dissociation reactions does not counteract the decrease in conductivity caused by the dilution of the solution, since the ionic conductivity of Na$^+$ ions is approximately 7 times smaller than that of H$^+$ ions, and it is also smaller than the

Fig. 8. Evolution of the permselective factor between nitrate ions and citrate species ($P_{Cit^{3-}}^{NO_3^-}$) at different current densities for (a) mixtures of 0.1 M H$_3$Cit + 0.015 M NaNO$_3$ and (b) mixtures of 0.1 M Na$_3$Cit + 0.015 M NaNO$_3$.
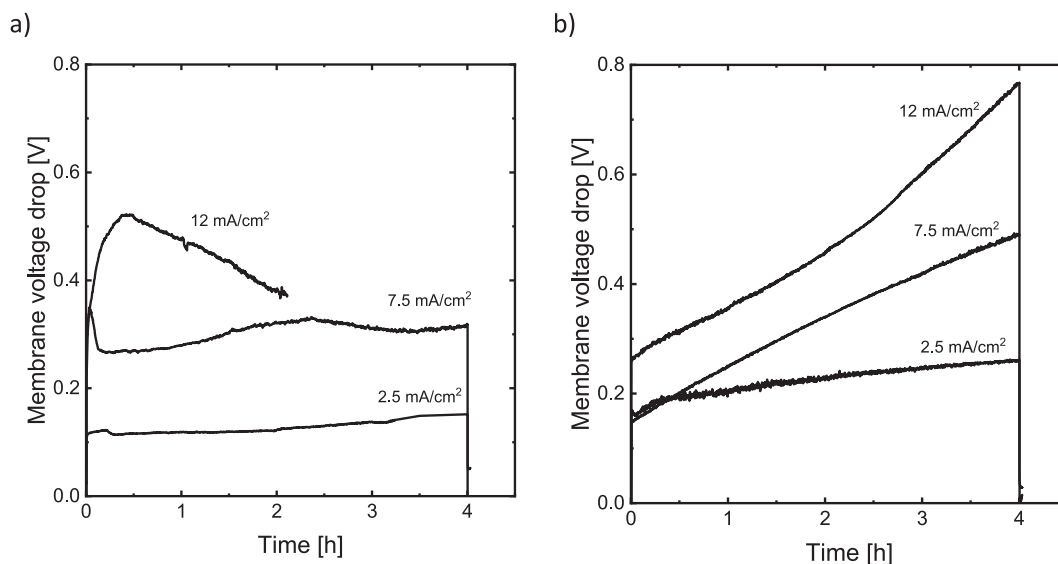
a)

b)

Fig. 9. Evolution of the membrane voltage drop at different current densities for (a) mixtures of 0.1 M H_3Cit + 0.015 M $NaNO_3$ and (b) mixtures of 0.1 M Na_3Cit + 0.015 M $NaNO_3$.

The selective transport of nitrate ions versus citrates can be better studied analyzing the evolution of the permselectivity factor for each experimental condition. Fittings of the evolution of C/C_0 for nitrates and citrates were obtained for each experiment, and the permselectivity factor ($P_{Cit^{3-}}^{NO_3^-}$) was calculated from the derivatives with time of the fittings (Eqs. (2) and (3)). The evolution of permselectivity factor is presented in Fig. 8 for all ED experiments conducted with the mixtures. The most remarkable result is that selectivity towards nitrate ions is higher than 1 in every moment for all solutions and current densities. However, it has the highest values during the first stages of the ED experiments, and then decays with time. This gradual decrease in permselectivity until a stable value is reached may be related to the changing trend in the concentration of both species. At the beginning of the experiments, the concentration of NO_3^- ions decreases fast until an asymptotic trend in C/C_0 for nitrate ions is reached; at that moment the transport of citrate species becomes faster, thus coinciding with the stabilization of the selectivity factors at the end of the experiments. In any case, given the high values of $P_{Cit^{3-}}^{NO_3^-}$, the most feasible strategy for the separation of both species is to promote the removal of the inorganic anions from the fermenters.

Regarding the effect of pH on selectivity, in general, the selective transport of nitrates over citrate species is slightly larger at pH 2, which can be related with the predominance of NO_3^- as anions in the solution. The highest permselectivity factor is obtained for the 0.1 M H_3Cit + 0.015 M $NaNO_3$ system under the application of 2.5 mA/cm² during the initial stages of the ED process with a value of 95. For this system, the steady value of permselectivity is reached after 1 h with a value of 20. For the system at pH 8 (0.1 M Na_3Cit + 0.015 M $NaNO_3$), a similar trend is observed, and the highest permselectivity factor is also obtained at the beginning of the experiments for the lowest applied current density, with a value of 58, which then gets stable for longer times around a value of 22. The permselectivity achieved in this study at 2.5 mA/cm² is significantly higher than values reported in previous studies dealing with the separation of inorganic and organic anions; Melnikov et al. achieved a specific permselectivity coefficient around 5 in the separation of chloride and acetate anions [17]. They also observed that the highest values of permselectivity were achieved at low applied current densities. The reason behind the high values achieved in the present work may be related to the fact that citrate anions are trivalent, thus their transport through the anion-exchange membrane may be delayed by the stronger interactions with the fixed ion-exchange groups of the

membrane. Another factor that may affect such differences in membrane selectivity is the type of membrane. The AMV-N membrane is homogeneous, thus, the absence of interstices between reinforcing meshes and ion conducting sites may enhance the intrinsic selectivity of the membrane material.

The highest selectivity is obtained in both systems at the lowest values of current density, which is consistent with the association of the i_{lim} values in the current–voltage curves with the depletion of nitrate ions. These results confirm that the transport of NO_3^- ions takes place more preferentially at low current densities, when their transport from the bulk solution towards the membrane surface is fast enough to satisfy the imposed charge transfer through the membranes. At larger current densities, the transport of nitrate ions becomes limited by diffusion and the dissociation of the different species of citric acid and sodium citrate into Cit^{3-} ions is triggered. The effect of pH on ion transport selectivity is more noticeable at high current densities, where the availability of nitrate ions at the depleting membrane surface is lower.

The evolution of the membrane voltage drop for the ED with the mixtures is shown in Fig. 9. Differing from the evolutions obtained at the two pH values with single salt/acid solutions, the initial values registered with the mixtures are quite similar, which is in agreement with the important contribution of $NaNO_3$ to the solution conductivity, as reported in Table 2. The trends obtained with the mixtures with H_3Cit are also consistent with the regime of the current–voltage curves corresponding to each applied current density. For 2.5 and 7.5 mA/cm², this system is operating in the underlimiting range of currents, so that the membrane voltage drop does not increase significantly during the experiment. However, for 12 mA/cm², the voltage drop increases fast during the first stages of the ED, and then decreases until the end of the experiment. This evolution is similar to that observed with single salt solutions of H_3Cit, and hence, indicates that the limited transfer of anions from the bulk towards the membrane surface triggers ampholytic reactions of citric acid, what increases the conductivity of the electrolyte layers in the vicinities of the membrane.

The evolution of membrane voltage drop obtained with the mixtures with Na_3Cit is also in good agreement with the regions corresponding to each applied current density: underlimiting, plateau and overlimiting region of currents. At the lowest value of 2.5 mA/cm², the voltage drop remains around a value of 0.2 V, whereas it increases faster with the applied current for the other two current densities. This evolution of membrane voltage exhibiting a continued increase with time would be also expected for strong electrolytes. In this case, the concentration of
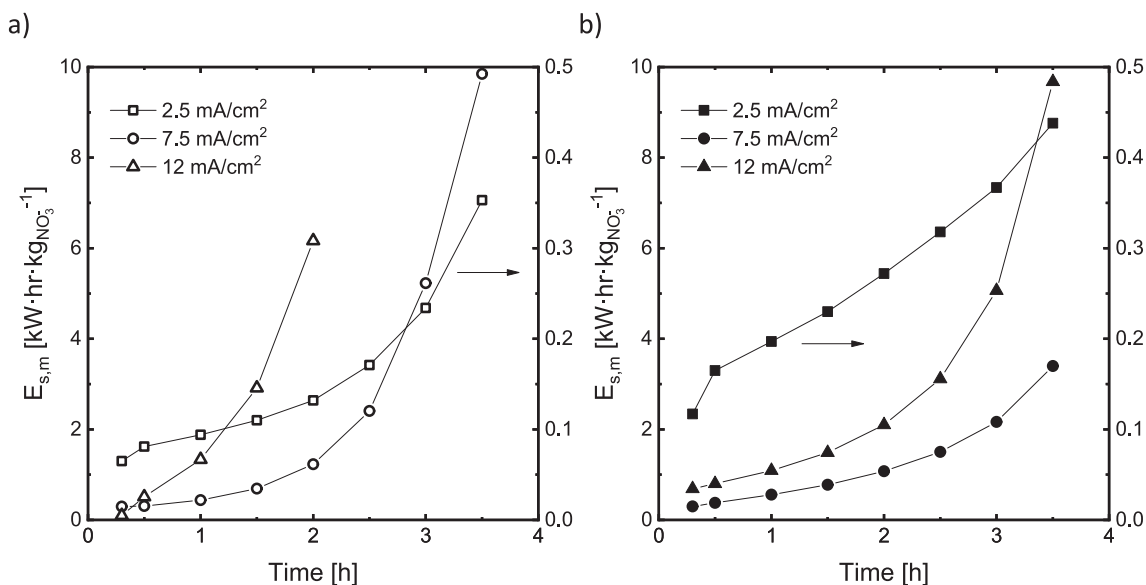
Fig. 10. Evolution of the specific energy consumption for the transport of nitrates in the membrane region for (a) mixtures of 0.1 M H_3Cit + 0.015 M $NaNO_3$ and (b) mixtures of 0.1 M Na_3Cit + 0.015 M $NaNO_3$.

citrate anions is higher, the neutral species H_3Cit or Na_3Cit do not accumulate next to the membrane surface, and their dissociation is not relevant during the experiment. As a consequence, the evolution of membrane voltage drop for this system is similar to that expected for strong electrolytes: it increases as the depletion of ionic species next to the dilute membrane surface takes place. It must be also mentioned that the pH in the bulk solution of the central compartments did not change significantly during the experiments, as reported in Table A.1 of the Appendix. This would indicate that the dissociation of citrate species should take place mainly in the solution layer next to the membranes.

The specific energy consumption for the separation process was calculated per mass of NO_3^- ions recovered, given the fact that the most feasible separation of both species is achieved via the removal of these more mobile ions through the anion-exchange membrane. In spite of the different speciation of both types of solutions, the results of specific energy consumption are very similar in both cases (Fig. 10). The best operating conditions for the separation of citrates and nitrates are attained with the lowest applied current density of 2.5 mA/cm², with final $E_{s,m}$ values of 0.35 and 0.44 kW·hr/kg_{NO3-} at pH 2 and 8, respectively. In general, at the beginning of the ED operation, the best results are achieved with the mixtures of H_3Cit and $NaNO_3$ (pH 2). This could be explained by the fact that the conductivity of the solutions with the mixtures is similar, and by the higher selectivity toward nitrate ions at low pH values, where the availability of anions of citric acid is scarcer. With the progress of ED, the dissociation of H_3Cit activates the transport of citrates through the membranes, produces a drop in the selectivity towards nitrate ions, and contributes to increase the specific energy consumption for the separation of nitrates.

4. Conclusions

In the present work, the challenge of separating organic and inorganic species is addressed for the specific application of citric acid purification by means of ED. Different parameters of the process have been investigated, i.e. the applied current density, the pH of the solutions, and the electrolyte concentration. The progress of the ED separation has been evaluated in terms of selectivity of anion transport, evolution of membrane voltage drops and energy consumption for the separation of nitrate ions from fermentation broths. A first characterization by means of chronopotentiometry reveals significant differences in ion transport depending on the pH of the solutions, which are attributed to changes in

the speciation of anionic species. In the absence of $NaNO_3$, at low pH values, the current–voltage curves show a constant and high resistance over a wide range of current densities. At high pH values, the resistance of the membrane system is higher at low current densities and decreases at high current densities. This unexpected behavior is attributed to the dissociation of neutral citric acid molecules, which takes place when high current densities are imposed. The dissociation reactions are also identified in chronopotentiometric curves by an initial peak in voltage drop which is followed by a gradual decrease as new ionic species are generated as a result of ampholytic reactions. On the contrary, the current–voltage curves of mixtures with $NaNO_3$ include three characteristic regions: the quasi-ohmic, the plateau and the overlimiting region.

ED experiments of longer duration resulted useful for identifying long-term phenomena that was imperceptible by means of chronopotentiometry. In the absence of inorganic anions, the transport of citrates in galvanostatic mode is practically independent of the pH of the solutions, however, the membrane voltage drop is higher at low pH due to the higher concentration of the undissociated form of citric acid. In general, all conditions evaluated resulted in a preferential transport of nitrates over citrates through the membranes. Nonetheless, the highest separation efficiency between nitrates and citrates is achieved in the underlimiting range of currents, where dissociation reactions involving citric acid are less relevant. It is possible to remove nitrates from the fermentation broths without implying a significant loss of the produced organic acid. Such conditions also lead to the lowest specific energy consumption (< 0.5 $kW·hr·kg_{NO_3^-}^{-1}$). The results obtained in the present study demonstrate that ED is a feasible option for removing inorganic ions from fermentation broths; however, further studies with real solutions are encouraged in subsequent research steps.

Declaration of competing interest

The authors declare that they have no known competing financial interests or personal relationships that could have appeared to influence the work reported in this paper.
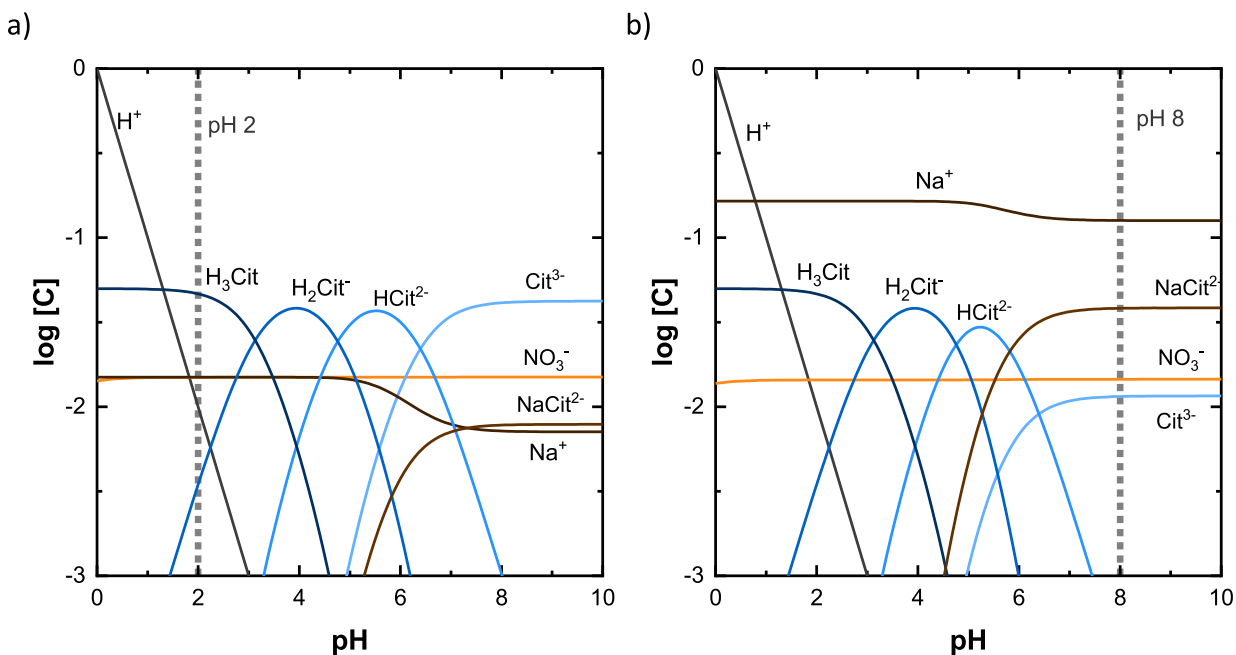
Appendix

a)

b)

Fig. A1. Logarithmic concentration diagram for a) mixtures of 0.05 M H_3Cit and 0.015 M $NaNO_3$, and b) mixtures of 0.05 M Na_3Cit and 0.015 M $NaNO_3$.
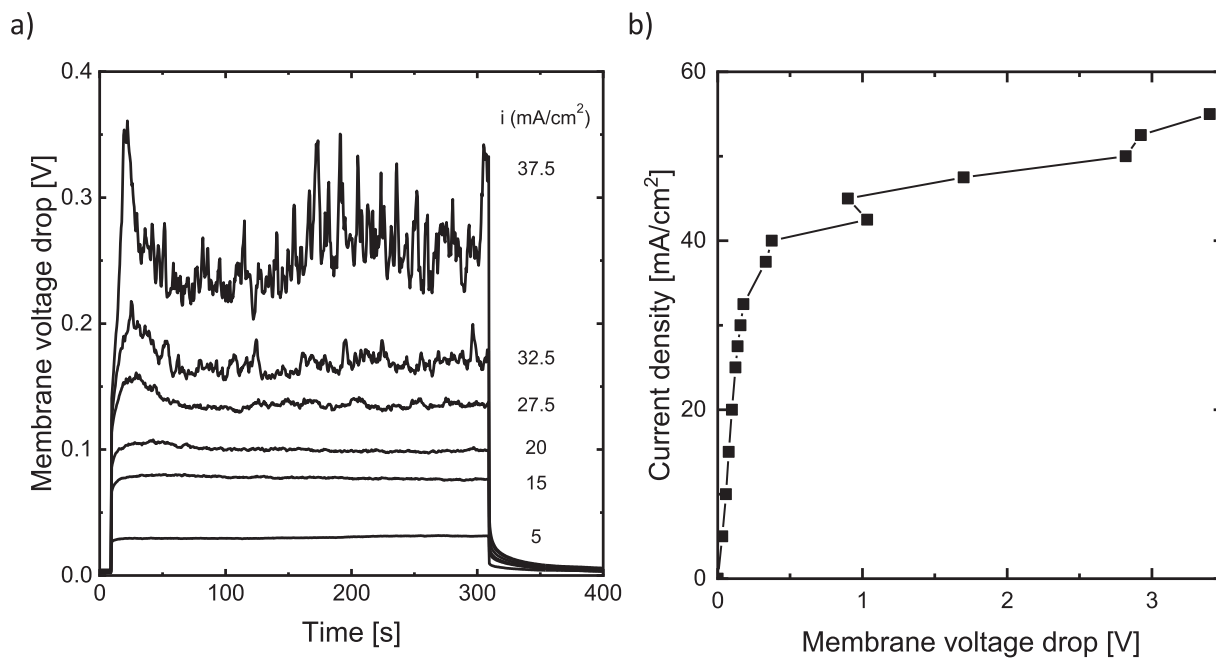
a)

b)

Fig. A2. a) Chronopotentiometric curve and b) current voltage curve obtained with the AMV-N anion-exchange membrane and 0.1 M NaCl solutions.
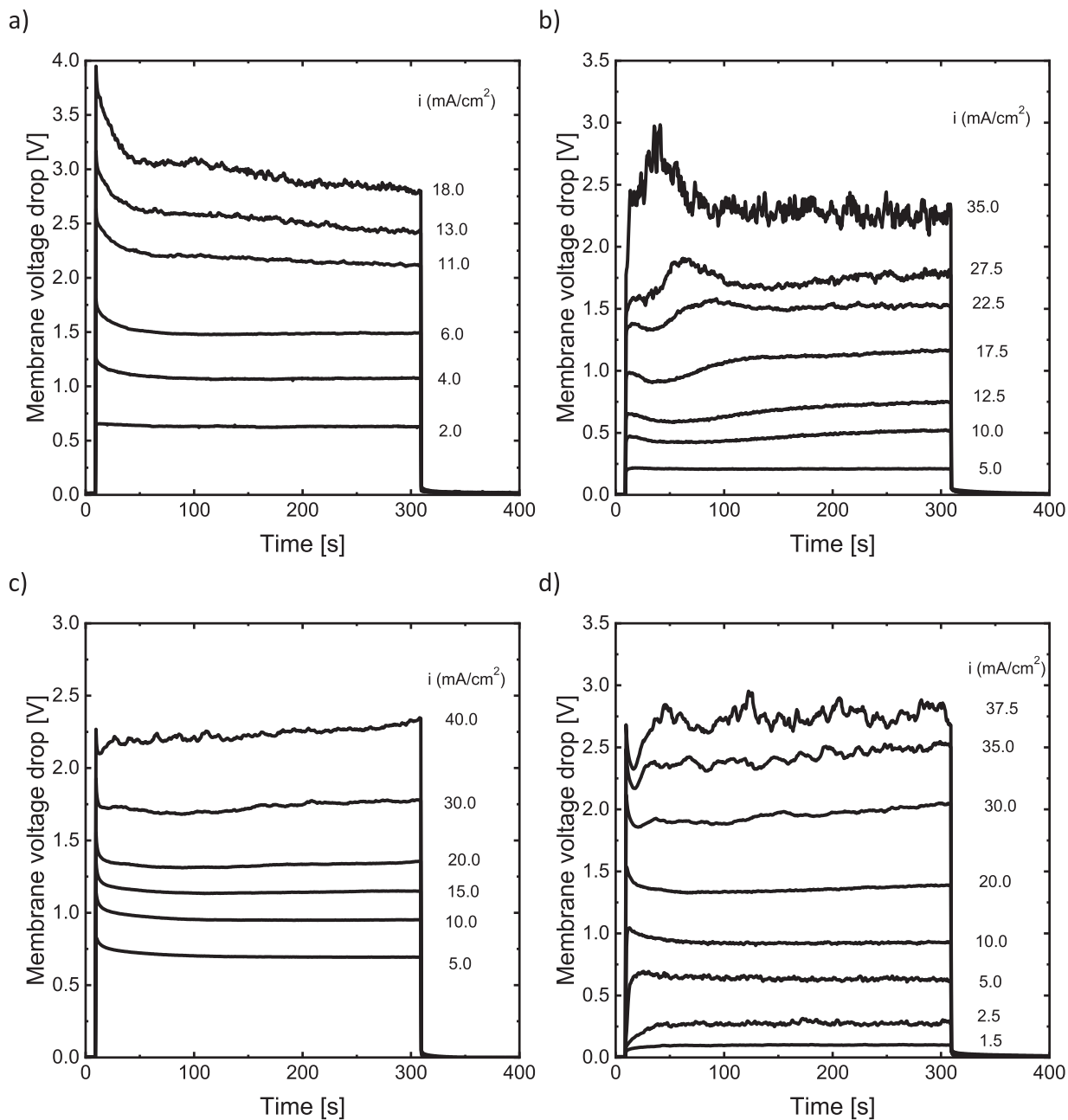
Fig. A3. Chronopotentiometric curves obtained with a) 0.05 M H_3Cit, b) mixtures of 0.05 M H_3Cit 0.1 M and 0.015 M $NaNO_3$, c) 0.05 M Na_3Cit, and d) mixtures of 0.05 M Na_3Cit and 0.015 M $NaNO_3$.
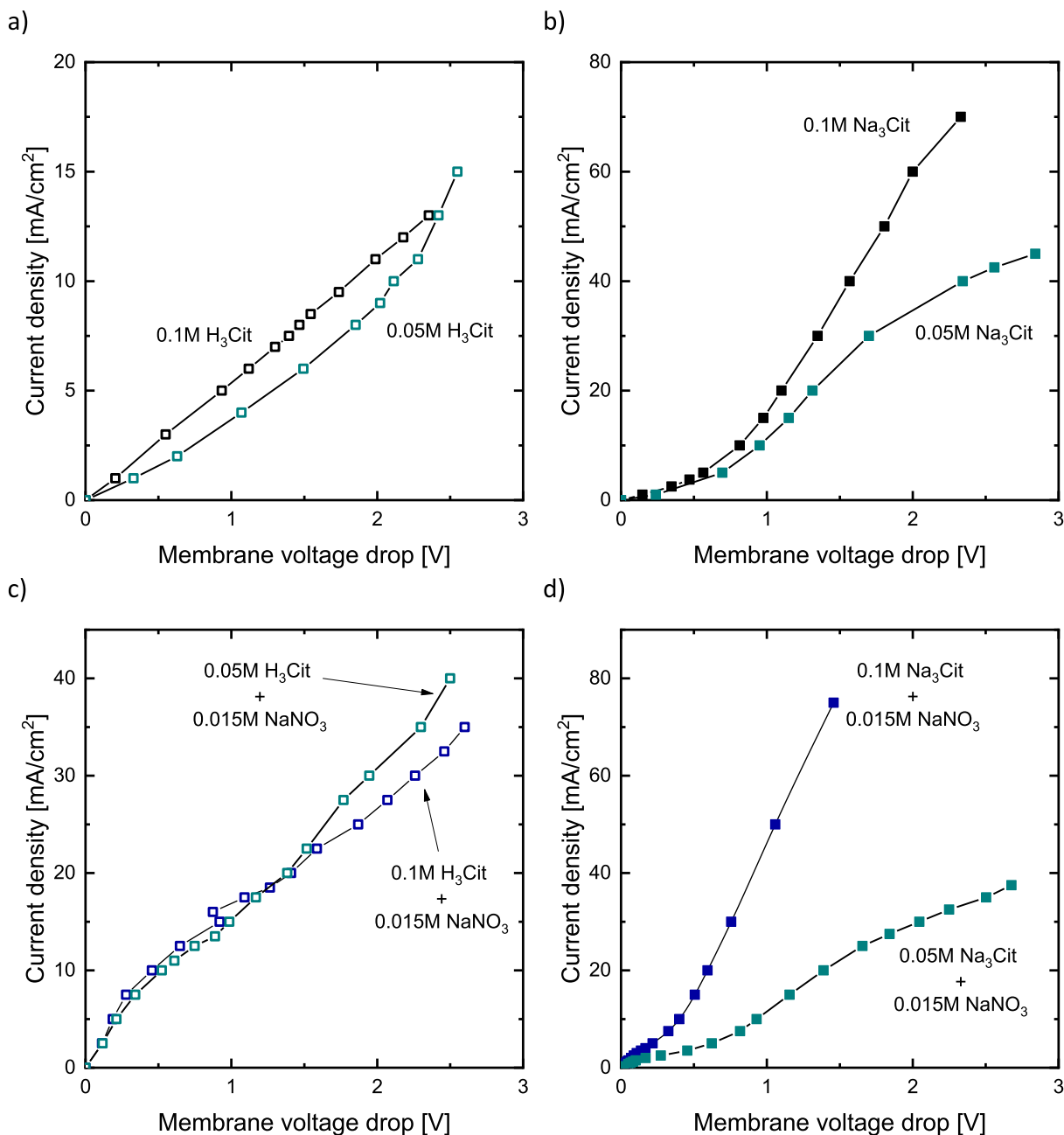
Fig. A4. Comparison between the currentvoltage curves obtained with citrate solutions at total citrate concentrations of 0.1 and 0.05 M. a) Comparison between acidic solutions, b) comparison between salt solutions, c) comparison between acidic solutions mixed with $NaNO_3$, and d) comparison between salt solutions mixed with $NaNO_3$.

Table A1
Initial and final values of conductivity and pH in the central compartments of the ED cell for each of the long-term experiments.

Solution	i (mA/cm²)	Initial conductivity (mS/cm)	Final conductivity (mS/cm)	Initial pH	Final pH
0.1 M H$_3$Cit	7.5	3.35	3.27	2.09	2.02
0.1 M Na$_3$Cit	7.5	18.31	15.15	8.44	10.07
0.1 M H$_3$Cit + 0.015 M NaNO$_3$	2.5	1.355	1.225	2.03	1.92
	7.5	4.72	2.54	1.89	2.01
	12	4.26	2.81	2.13	1.99
0.1 M Na$_3$Cit + 0.015 M NaNO$_3$	2.5	17.03	18.31	7.95	8.03
	7.5	17.03	15.72	7.95	9.85
	12	17.03	12.18	7.43	10.13

References

[1] J. Son, J.C. Joo, K.A. Baritugo, S. Jeong, J.Y. Lee, H.J. Lim, S.H. Lim, J.I. Yoo, S. J. Park, Consolidated microbial production of four-, five-, and six-carbon organic acids from crop residues: current status and perspectives, Bioresour. Technol. 351 (2022) 127001, https://doi.org/10.1016/j.biortech.2022.127001.

[2] F.H. Isikgor, C.R. Becer, Lignocellulosic biomass: a sustainable platform for the production of bio-based chemicals and polymers, Polym. Chem. 6 (2015) 4497–4559, https://doi.org/10.1039/c5py00263j.

[3] M. Alexandri, R. Schneider, H. Papapostolou, D. Ladakis, A. Koutinas, J. Venus, Restructuring the conventional sugar beet industry into a novel biorefinery: fractionation and bioconversion of sugar beet pulp into succinic acid and value-added coproducts, ACS Sustain. Chem. Eng. 7 (2019) 6569–6579, https://doi.org/10.1021/acssuschemeng.8b04874.

[4] B.C. Behera, R. Mishra, S. Mohapatra, Microbial citric acid: Production, properties, application, and future perspectives, Food Front. 2 (2021) 62–76, https://doi.org/10.1002/fft2.66.

[5] A. Amato, A. Becci, F. Beolchini, Citric acid bioproduction: the technological innovation change, Crit. Rev. Biotechnol. 40 (2020) 199–212, https://doi.org/10.1080/07388551.2019.1709799.

[6] A.J.J. Straathof, The proportion of downstream costs in fermentative production processes, Comprehensive Biotechnology, Second Edition 2 (2011) 811–814, https://doi.org/10.1016/B978-0-08-088504-9.00492-X.

[7] Q.Z. Li, X.L. Jiang, X.J. Feng, J.M. Wang, C. Sun, H.B. Zhang, M. Xian, H.Z. Liu, Recovery processes of organic acids from fermentation broths in the biomass-based industry, J. Microbiol. Biotechnol. 26 (2015) 1–8, https://doi.org/10.4014/jmb.1505.05049.

[8] J. Wang, Z. Cui, Y. Li, L. Cao, Z. Lu, Techno-economic analysis and environmental impact assessment of citric acid production through different recovery methods, J. Clean. Prod. 249 (2020) 119315, https://doi.org/10.1016/j.jclepro.2019.119315.

[9] C. Jiang, Y. Wang, T. Xu, Membranes for the recovery of organic acids from fermentation broths, in: Membrane Technologies for Biorefining, Woodhead Publishing, 2016, pp. 135–161.

[10] S.J. Andersen, T. Hennebel, S. Gildemyn, M. Coma, J. Desloover, J. Berton, J. Tsukamoto, C. Stevens, K. Rabaey, Electrolytic membrane extraction enables production of fine chemicals from biorefinery sidestreams, Environ. Sci. Tech. 48 (2014) 7135–7142, https://doi.org/10.1021/es500483w.

[11] T. Rózsenberszki, P. Komáromy, É. Hülber-Beyer, A. Pesti, L. Koók, P. Bakonyi, K. Bélafi-Bakó, N. Nemestóthy, Bipolar membrane electrodialysis integration into the biotechnological production of itaconic acid: a proof-of-concept study, Chem. Eng. Res. Des. 190 (2023) 187–197, https://doi.org/10.1016/j.cherd.2022.12.023.

[12] X. Ma, W. Liu, C. Li, Y. Dong, R. Zhou, Z. Dong, J. He, L. Sun, H. Yan, Bipolar membrane electrodialysis for efficient production of ferulic acid in alcohol/water mixed solvent, Sep. Purif. Technol. 341 (2024) 126876, https://doi.org/10.1016/j.seppur.2024.126876.

[13] P.A. Hernandez, M. Zhou, I. Vassilev, S. Freguia, Y. Zhang, J. Keller, P. Ledezma, B. Virdis, Selective Extraction of Medium-Chain Carboxylic Acids by Electrodialysis and Phase Separation (2021), https://doi.org/10.1021/acsomega.1c00397.

[14] P. Mandal, R. Mondal, P. Goel, E. Bhuvanesh, U. Chatterjee, S. Chattopadhyay, Selective recovery of carboxylic acid through PVDF blended anion exchange membranes using electrodialysis, Sep. Purif. Technol. 292 (2022), https://doi.org/10.1016/j.seppur.2022.121069.

[15] K. Prochaska, M.J. Woźniak-Budych, Recovery of fumaric acid from fermentation broth using bipolar electrodialysis, J. Membr. Sci. 469 (2014) 428–435, https://doi.org/10.1016/j.memsci.2014.07.008.

[16] J. Liu, J. Liang, X. Feng, W. Cui, H. Deng, Z. Ji, Y. Zhao, X. Guo, J. Yuan, Effects of inorganic ions on the transfer of weak organic acids and their salts in electrodialysis process, J. Membr. Sci. 624 (2021) 119109, https://doi.org/10.1016/j.memsci.2021.119109.

[17] S.S. Melnikov, E.N. Nosova, E.D. Melnikova, V.I. Zabolotsky, Reactive separation of inorganic and organic ions in electrodialysis with bilayer membranes, Sep. Purif. Technol. 268 (2021) 118561, https://doi.org/10.1016/j.seppur.2021.118561.

[18] S. Melnikov, D. Kolot, E. Nosova, V. Zabolotskiy, Peculiarities of transport-structural parameters of ion-exchange membranes in solutions containing anions of carboxylic acids, J. Membr. Sci. 557 (2018) 1–12, https://doi.org/10.1016/j.memsci.2018.04.017.

[19] A. Luiz, E. Spencer, D.D. McClure, H.G.L. Coster, G.W. Barton, J.M. Kavanagh, Membrane selection for the desalination of bio-refinery effluents using electrodialysis, Desalination 428 (2018) 1–11, https://doi.org/10.1016/j.desal.2017.11.006.

[20] H. Zhou, P. Ju, S. Hu, L. Shi, W. Yuan, D. Chen, Y. Wang, S. Shi, Separation of hydrochloric acid and oxalic acid from rare earth oxalic acid precipitation mother liquor by electrodialysis, Membranes 13 (2023), https://doi.org/10.3390/membranes13020162.

[21] J. Lin, W. Ye, S. Xie, J. Du, R. Liu, D. Zou, X. Chen, Z. Yu, S. Fang, E.Y.M. Ang, W. Toh, D.D. Han, T.Y. Ng, D.H. Seo, S. Zhao, B. Van der Bruggen, M. Xie, Y.M. Lee, Shielding effect enables fast ion transfer through nanoporous membrane for highly energy-efficient electrodialysis, Nat. Water. 1 (2023) 725–735, https://doi.org/10.1038/s44221-023-00113-5.

[22] N. Kim, J. Lee, X. Su, Precision tuning of highly selective polyelectrolyte membranes for redox-mediated electrochemical separation of organic acids, Adv. Funct. Mater. 33 (2023), https://doi.org/10.1002/adfm.202211645.

[23] A.D. Gorobchenko, S.A. Mareev, O.A. Rybalkina, K.A. Tsygurina, V.V. Nikonenko, N.D. Pismenskaya, How do proton-transfer reactions affect current-voltage characteristics of anion-exchange membranes in salt solutions of a polybasic acid? Modeling and experiment, J. Membr. Sci. 683 (2023) 121786, https://doi.org/10.1016/j.memsci.2023.121786.

[24] A. Gorobchenko, O. Yurchenko, S. Mareev, C. Zhang, N. Pismenskaya, V. Nikonenko, Study of non-stationary phosphorus transport with phosphoric acid anions through an anion-exchange membrane by chronopotentiometry: experiments and modeling, J. Water Process Eng. 64 (2024) 105711, https://doi.org/10.1016/j.jwpe.2024.105711.

[25] E.H. Rotta, M.C. Martí-Calatayud, V. Pérez-Herranz, A.M. Bernardes, Evaluation by means of electrochemical impedance spectroscopy of the transport of phosphate ions through a heterogeneous anion-exchange membrane at different ph and electrolyte concentration, Water. 15 (2023).

[26] Y. Wang, N. Zhang, C. Huang, T. Xu, Production of monoprotic, diprotic, and triprotic organic acids by using electrodialysis with bipolar membranes: effect of cell configurations, J. Membr. Sci. 385–386 (2011) 226–233, https://doi.org/10.1016/j.memsci.2011.09.044.

[27] H. Luo, X. Cheng, G. Liu, Y. Zhou, Y. Lu, R. Zhang, X. Li, W. Teng, Citric acid production using a biological electrodialysis with bipolar membrane, J. Membr. Sci. 523 (2017) 122–128, https://doi.org/10.1016/j.memsci.2016.09.063.

[28] S. Mores, L.P. de S. Vandenberghe, A.I. Magalhães Júnior, J.C. de Carvalho, A.F. M. de Mello, A. Pandey, C.R. Soccol, Citric acid bioproduction and downstream processing: status, opportunities, and challenges, Bioresour. Technol. 320 (2021), https://doi.org/10.1016/j.biortech.2020.124426.

[29] J.C.E. Francisco, W.L. Rivera, P.G. Vital, Influences of carbohydrate, nitrogen, and phosphorus sources on the citric acid production by fungal endophyte Aspergillus fumigatus P3I6, Prep. Biochem. Biotech. 50 (2019) 292–301.

[30] E. Carsanba, S. Papanikolaou, P. Fickers, H. Erten, Screening various Yarrowia lipolytica strains for citric acid production, Yeast 36 (2019) 319–327, https://doi.org/10.1002/yea.3389.

[31] J. Pietkiewicz, M. Janczar, The effect of nitrogen in the fermentation broth on citric acid production by Aspergillus niger, Food Biotechnol. 17 (2000) 241–245.

[32] E. Papadaki, F.T. Mantzouridou, Citric acid production from the integration of Spanish-style green olive processing wastewaters with white grape pomace by Aspergillus niger, Bioresour. Technol. 280 (2019) 59–69, https://doi.org/10.1016/j.biortech.2019.01.139.

[33] D. Harvey, Modern Analytical Chemistry, McGraw-Hill, New York, 2000.

[34] X.T. Le, Contribution to the study of properties of Selemion AMV anion exchange membranes in acidic media, Electrochim. Acta 108 (2013) 232–240, https://doi.org/10.1016/j.electacta.2013.07.011.

[35] M.C. Martí-Calatayud, M. García-Gabaldón, V. Pérez-Herranz, E. Ortega, Determination of transport properties of Ni(II) through a Nafion cation-exchange membrane in chromic acid solutions, J. Membr. Sci. 379 (2011) 449–458, https://doi.org/10.1016/j.memsci.2011.06.014.

[36] M.C. Martí-Calatayud, M. García-Gabaldón, V. Pérez-Herranz, S. Sales, S. Mestre, Synthesis and electrochemical behavior of ceramic cation-exchange membranes based on zirconium phosphate, Ceram. Int. 39 (2013) 4045–4054, https://doi.org/10.1016/j.ceramint.2012.10.255.

[37] K.S. Barros, M.C. Martí-Calatayud, T. Scarazzato, A.M. Bernardes, D.C.R. Espinosa, V. Pérez-Herranz, Investigation of ion-exchange membranes by means of chronopotentiometry: a comprehensive review on this highly informative and multipurpose technique, Adv. Colloid Interface Sci. 293 (2021) 102439, https://doi.org/10.1016/j.cis.2021.102439.

[38] S. Abdu, M.C. Martí-Calatayud, J.E. Wong, M. García-Gabaldón, M. Wessling, Layer-by-layer modification of cation exchange membranes controls ion selectivity and water splitting, ACS Appl. Mater. Interfaces 6 (2014) 1843–1854, https://doi.org/10.1021/am4048317.

[39] V.D. Titorova, S.A. Mareev, A.D. Gorobchenko, V.V. Gil, V.V. Nikonenko, K. G. Sabbatovskii, N.D. Pismenskaya, Effect of current-induced coion transfer on the shape of chronopotentiograms of cation-exchange membranes, J. Membr. Sci. 624 (2021) 119036, https://doi.org/10.1016/j.memsci.2020.119036.

[40] M.C. Martí-Calatayud, M. García-Gabaldón, V. Pérez-Herranz, Mass transfer phenomena during electrodialysis of multivalent ions: chemical equilibria and overlimiting currents, Appl. Sci. (Switzerland). 8 (2018) 1566, https://doi.org/10.3390/app8091566.

[41] L. Hernández-Pérez, M.C. Martí-Calatayud, M.T. Montañés, V. Pérez-Herranz, Interplay between forced convection and electroconvection during the overlimiting ion transport through anion-exchange membranes: a Fourier transform analysis of membrane voltage drops, Membranes 13 (2023), https://doi.org/10.3390/membranes13030363.

[42] N. Pismenskaya, O. Rybalkina, I. Moroz, S. Mareev, V. Nikonenko, Influence of electroconvection on chronopotentiograms of an anion-exchange membrane in solutions of weak polybasic acid salts, Int. J. Mol. Sci. 22 (2021) 25–27, https://doi.org/10.3390/ijms222413518.

[43] J. Stodollick, R. Femmer, M. Gloede, T. Melin, M. Wessling, Electrodialysis of itaconic acid: a short-cut model quantifying the electrical resistance in the

overlimiting current density region, J. Membr. Sci. 453 (2014) 275–281, https://doi.org/10.1016/j.memsci.2013.11.008.

[44] H.P. Gregor, I.F. Miller, Field-induced dissociation at the ion-selective membrane-solution interface, J. Am. Chem. Soc. 86 (1964) 5689–5690.

[45] A. Tanioka, M. Kawaguchi, M. Hamada, K. Yoshie, Dissociation constant of a weak electrolyte in charged membrane, J. Phys. Chem. B 102 (1998) 1730–1735, https://doi.org/10.1021/jp972900g.

[46] M.C. Martí-Calatayud, E. Evdochenko, J. Bär, M. García-Gabaldón, M. Wessling, V. Pérez-Herranz, Tracking homogeneous reactions during electrodialysis of organic acids via EIS, J. Membr. Sci. 595 (2020) 117592, https://doi.org/10.1016/j.memsci.2019.117592.

[47] D.R. Lide, CRC Handbook of Chemistry and Physics, 70th ed., CRC Press Inc., Boca Raton, 2009.